Iron coral

Li, Qianwei; Liu, Daoqing; Wang, Tongzhe; Chen, Chunmao; Gadd, Geoffrey Michael

Published in:
Chemical Engineering Journal

DOI:
10.1016/j.cej.2020.126263

Publication date:
2020

Iron coral: novel fungal biomineralization of nanoscale zerovalent iron composites for treatment of chlorinated pollutants

Qianwei Li[1‡], Daoqing Liu[2,3‡],Tongzhe Wang[1], Chunmao Chen[1], and Geoffrey Michael Gadd[1,4]*

[1]State Key Laboratory of Heavy Oil Processing, State Key Laboratory of Petroleum Pollution Control, China University of Petroleum-Beijing, Beijing 102249, China

[2]Department of Environmental Engineering, Peking University, Beijing 100871, China

[3]The Key Laboratory of Water and Sediment Sciences, Ministry of Education, Beijing 100871, China

[4]Geomicrobiology Group, School of Life Sciences, University of Dundee, Dundee DD1 5EH, Scotland, UK

*Corresponding author: Chunmao Chen, chunmaochan@163.com

[‡]both authors contributed equally to this work.

Key words: fungal biomineralization; nZVI, chlorinated pollution; geochemical simulation

Abstract

In this research, a facile fungal biomineralization method was developed for the synthesis of nanoscale zerovalent iron (nZVI) with a unique N-doped branching structure, which showed excellent stability and mediated high degradation of carbon tetrachloride (CCl_4) in aqueous solution. The ureolytic fungus *Neurospora crassa* was cultured in medium containing Fe^{2+} and urea which resulted in iron carbonate biomineral precipitation. Following carbonization at 900^oC, the fungal-carbonate composite became highly porous and granular nanoparticles (~50 nm diameter) were distributed evenly around the carbonized hyphae in a coralline manner. This 'iron coral' composite was identified as a mixture of zerovalent iron (Fe^0), carbon iron ($Fe_{1.91}C_{0.09}$) and iron oxide (Fe_3O_4). The porous branching hyphal framework improved the capture efficiency of CCl_4, and the N-doped sites may accelerate the electron transfer between CCl_4 and nZVI. Geochemical simulation was applied to verify the formation of the biominerals, and chemical analyses confirmed its significant degradation ability for CCl_4. These findings have therefore demonstrated that ureolytic fungi can provide a promising environmental-friendly system for the novel preparation of nZVI through biomineralization with the resulting 'iron coral' capable of significant removal of a chlorinated compound and therefore indicating new bioremediation applications.

1. Introduction

Chlorinated pollutants are the most common organic pollutants in groundwater which can cause serious problems for ecosystems and human health due to their volatility, carcinogenic effects and bioaccumulation potential [1]. Over the last three decades, zerovalent iron (ZVI) has been extensively applied for the remediation or removal of chlorinated substances, including hydrocarbons, from contaminated aqueous solution [2-5]. ZVI technology research has been mainly focused in three contexts: development of various synthesis methods to overcome limitations of ZVI during remediation applications; exploring the possibility of ZVI for the removal of novel contaminants arising from modern industrial and agricultural technologies; and practical applications of ZVI in contaminated sites [1, 5, 6]. Although ZVI can exhibit excellent performance in contaminant removal, nanoscale ZVI (nZVI) particles offer a much higher potential due to their large specific surface area, high reactivity and adequate mobility [7, 8]. However, nanoscale particles tend to aggregate due to weak van der Waals forces, high surface energy and intrinsic magnetic interactions which results in a decrease in the number of active sites and reduced mobility thus limiting reaction efficiency and practical applications [4].

To improve dispersion and avoid nanoparticle aggregation, research has been carried out on the synthesis of novel nZVI-based materials, including surface modified nZVI (e.g., by chitosan or carboxyl methylated cellulose coatings and amino-functionalized nZVI) [8-10] and solid materials supporting nZVI (e.g., activated carbon, graphene and organic resins) [2, 11, 12]. A novel stabilized nZVI-Ni catalyst was developed using polyvinylpyrrolidone (PVP) and this exhibited better mobility than bare nZVI-Ni [13]. The stabilized nZVI-Ni could degrade trichloroethylene (TCE) completely in 1 h with superior dechlorination kinetics. Carbon-based materials, e.g. activated carbon, graphene, and carbon nanotubes, have been evaluated as important supporting materials for nZVI due to their high surface area, gap structure and other

unique properties [14]. Graphene-supported nZVI (G-nZVI) was prepared for the removal of trichlorinitromethane (TGNM) from drinking water and 99% of TGNM was adsorbed and degraded using a 60 mg l^{-1} G-nZVI dosage within 120 min [15]. Although stabilized and solid supported nZVI can exhibit high dispersibility and reactivity, several stabilizing agents have been reported to compete for nZVI active sites with contaminants while a stable distribution of nZVI on solid supports is hard to achieve [4, 16].

In the natural environment, fungi can interact with metal and minerals through various biomineralization, biosorption and biotransformation processes, which can be key components of biogeochemical cycles [17-20]. Biomineralization is the process of mineral formation by organisms and the final products commonly contain organic and inorganic components [17, 19]. One mechanism for the biomineralization of metal carbonates is related to urea degradation. In a growth medium or habitat containing urea, ureolytic microorganisms degrade urea and release ammonium (NH_4^+) and carbonate (CO_3^{2-}) ions, the latter reacting with free metal ions resulting in the precipitation of metal carbonates [17]. The surfaces of the branching mycelial network of filamentous fungi provide nucleation sites for mineral precipitation. Moreover, the secretion of metabolites (e.g. extracellular proteins, polysaccharides, amino acids, and organic acids) also play important roles in the formation of nano- and microscale minerals [21]. Previous research has demonstrated that the urease-positive fungi *Neurospora crassa*, *Pestalotiopsis* sp. and *Myrothecium gramineum* were able to precipitate toxic metal ions (e.g. Co^{2+}, Zn^{2+}, Cd^{2+}, Cu^{2+} and Ni^{2+}) as carbonates in a urea-modified medium[19, 22, 23]. It was shown that extracellular protein was responsible for governing mineral size and morphology and further studies proved that in the biomineralization process, the conformation of extracellular proteins preferentially formed β–structures rather than α-helixes [23]. Excreted amino acids, such as L-glutamic acid, were found to stabilize copper-containing minerals in the early stages of crystal growth and prevented crystal aggregation which resulted in the

bioprecipitation of nanoparticles [21]. Moreover, fungal biomass has been developed as a carbon precursor for various applications including electrochemical materials and electrocatalysis, through biomineralization and subsequent carbonization [22, 24]. In the process of biomineralization, the cross-linked branching hyphal structure can provide mechanical support and significant properties for the enhanced dispersion of reactants. The aim of this research was to examine the fungal biomineralization of nZVI by ureolytic fungi to provide understanding of the mechanisms involved and to identify possible applications for the degradation or bioremediation of chlorinated pollutants.

2. Materials and methods

2.1 Geochemical simulation of iron carbonate precipitation using Geochemist's Workbench (GWB)

Previous studies have demonstrated that ureolytic fungi can precipitate metal carbonates (e.g. $CaCO_3$, $SrCO_3$ and $CoCO_3$) in a carbonate-laden system produced by ureolysis [17-19, 21]. To understand the solubility of Fe^{2+} in the fungal biomineralization system, GWB 11.0.6 (Aqueous Solutions LLC, Urbana-Champaign, USA) was applied for the geochemical simulation of iron carbonate bioprecipitation, and this software can be used for the calculation of stability diagrams and determination of the chemical equilibrium states in aqueous solutions. Further details and application of the GWB software to examine carbonate bioprecipitation can be found in Li et al. [23]. In these experiments, the concentration of CO_3^{2-} was set as 330 mM (330 mM urea is completely degraded by ureolytic fungi incubated in AP1 media producing equimolar carbonate [23]) and the other set components were the same as in the AP1 medium (6.1 mM Cl^-, 0.83 mM SO_4^{2-}, 0.66 M NH_4^+, 4 mM K^+, 0.8 mM Mg^{2+}, 1.7 mM Na^+, 0.2 mM Ca^{2+}, 0.02 mM Mn^{2+}, 0.01 Mm Zn^{2+} and 9 μM Fe^{3+} at 25ºC). According to previous experimentation, the pH of fungal supernatants was between pH 7.0 and 8.0 after incubation in urea-containing media and therefore minerals precipitated in this pH range will be investigated in the simulation system.

2.2 Biomineralization of Fe-containing minerals by *Neurospora crassa*

The experimental fungus used was *Neurospora crassa* (WT ACCC #32256, Agricultural Culture Collection of China (ACCC), Beijing, China). It was grown in malt extract (ME) liquid medium in a shaking incubator in the dark (125 rpm, 25ºC). After 3 d incubation, fungal biomass was filtered using a sterilized sieve (80 mesh, i.e. 80 squares per linear inch, equivalent to squares of dimension 180 x 180 μm), resuspended in sterilized Milli-Q water and filtered

again. Fungal biomass was transferred to a modified liquid medium (AP1) for mineral precipitation. AP1 medium contained 111 mM glucose, 0.33 M urea, 4 mM K_2HPO_4, 0.8 mM $MgSO_4$, 0.2 mM $CaCl_2$, 2 mM NaCl and trace metals 1.4×10^{-2} mM $ZnSO_4$, 1.8×10^{-2} mM $MnSO_4$, and 1.6×10^{-3} mM $CuSO_4$. To obtain an appropriate amount of biominerals (iron carbonate) and ensure good growth of *N. crassa*, 10 and 20 mM Fe^{2+} were the final concentrations chosen for mineral precipitation in liquid medium. The $FeSO_4$ stock solutions (0.4 M) were filtered using 0.2 μm pore size membrane filters (Sartorius Stedim Biotech, Göttingen, Germany) prior to adding appropriate aliquots to the AP1 medium for the biomineralization experiments to achieve final concentrations of 10 and 20 mM $FeSO_4$. All experiments were conducted at least in triplicate.

2.3 Preparation of nZVI/fungal biomass composite

To prepare the nano zerovalent iron (nZVI)/fungal biomass composite, fungal biomass was collected after 6 d incubation in Fe-modified AP1 medium by centrifugation (4770 g x 20 min, 4°C), washed with Milli-Q water and dried in a vacuum freeze dryer (JOYN FD-1C-50, Shanghai, China) for several hours. The dried biomass was ground to a fine powder using an agate mortar and pestle and then put into a quartz boat. Carbonization of fungal biomass and the reduction of Fe^{2+} to Fe^0 were achieved by increasing the temperature to 900°C in a tube furnace (KejingOTF-1200X, Hefei, China) at a heating rate of 5°C min^{-1} which was then maintained for 1 h. Nitrogen gas was used to keep the atmosphere anaerobic during the whole process.

2.4 Characterization of minerals precipitated by *N. crassa*

Samples were fixed using 2.5% glutaraldehyde in 5 mM PIPES buffer (pH = 6.5) for 24 h at room temperature and then washed twice using the same PIPES buffer. Dehydration was

performed using vacuum freeze drying (SCIENTZ-10YG/A, Ningbo, China). Morphological and elemental analysis of fungal biomass before and after heat treatment were conducted using scanning electron microscopy (SEM) (ZEISS Gemini 300, Oberkochen, Germany) and energy dispersive X-ray analysis (EDXA) operating at voltages of 15 kV and 20 kV, respectively. The identification of biominerals was carried out using X-ray diffraction (XRD) (Bruker D8 Advance, Karlsruhe, Germany), Fourier transform infrared spectroscopy (FTIR) (Thermo Fisher 6700, Waltham, USA) and X-ray photoelectron spectroscopy (XPS) (Thermo Fisher, Waltham, MA, USA). Sample preparation and curve fitting analysis were conducted according to the procedures described in Li et al. [23].

After carbonization and reduction of Fe^{2+}, the surface properties and surface area of fungal biomass and the biogenic nZVI/fungal biomass composite were characterized by N_2 adsorption/desorption measurements using a surface area analyzer (Micromeritics ASAP 2020 HD88, Norcross, GA, USA). The thermal stability of the sample was investigated using thermogravimetric analysis-differential scanning calorimetry (TGA-DSC) (SDT Q600 V20.9 Build 20, TA instruments, DE, USA) in a nitrogen atmosphere (100 ml min^{-1}) from room temperature to 900^{o}C at a rate of 5^{o}C min^{-1}.

A 2 ml sample, from a 10% (*w/v*) solution in 10 ml MilliQ water, after heat treatment, was examined for stability using a LUMiSizer Dispersion Analyser (LUM GmbH, Berlin, Germany). The wavenumber for the space and time resolved extinction profiles (STEPTM) was 865 nm and the sedimentation speed was 4000 rpm. The transmitted light detector was used to scan along the height of the synthetic sample cell for 1 h.

2.5 Removal of carbon tetrachloride from solution by the 'iron coral' composite

For the degradation experiments, 0.1 g of biogenic nZVI/fungal biomass composite was added to 100 ml CCl_4 solution (16 mg l^{-1}, first dissolved in methanol) and kept in a shaking incubator

(125 rpm, 25^{o}C) for 150 min. The concentration of CCl_4 and the intermediate degradation products were measured every 30 min using a gas chromatography-mass spectrometer (GC-MS) (7890B-5977A, Agilent Technologies, CA, USA), and the selected ion monitoring (SIM) method of quantitation was selected.

2.6 Tafel scans of the 'iron coral' composite and commercial nZVI

To investigate the ability of iron coral to lose electrons, Tafel scans were performed on a CHI-660E electrochemical workstation fitted with a three electrode system enabling the free corrosion potentials to be recorded. Sample preparation was conducted according to the procedures described in Hu et al. [25].

3. Results

3.1 Characterization of the biogenic nZVI/fungal biomass composite 'iron coral'

The preparation of the biogenic nZVI/fungal biomass composite is illustrated in Fig. 1a. The ureolytic fungus was incubated in Fe-modified media to achieve biomineralization of Fe-containing minerals, followed by carbonization to obtain the biogenic nZVI/fungal biomass composite,which was subsequently applied for the degradation of CCl_4. The solubility and stability of Fe^{2+}, relevant Fe-containing minerals, and the predominance of aqueous Fe species were calculated individually in a simulated fungal growth supernatant system using GWB. The obtained results showed that siderite ($FeCO_3$) and vivianite ($Fe_3(PO_4)_2 \cdot 8H_2O$) were the main minerals in the simulated medium (Fig. 1b). Iron carbonate ($FeCO_3$) could precipitate over a range of pH 1 to 8.3 while the lowest concentration of Fe^{2+} for carbonate precipitation was around 0.32 μM (here, a (Fe^{2+}) was equal to Fe^{2+} concentration, log a (Fe^{2+}) ≈ -6.5, c (Fe^{2+}) ≈ a (Fe^{2+}) ≈ 0.32 μM).

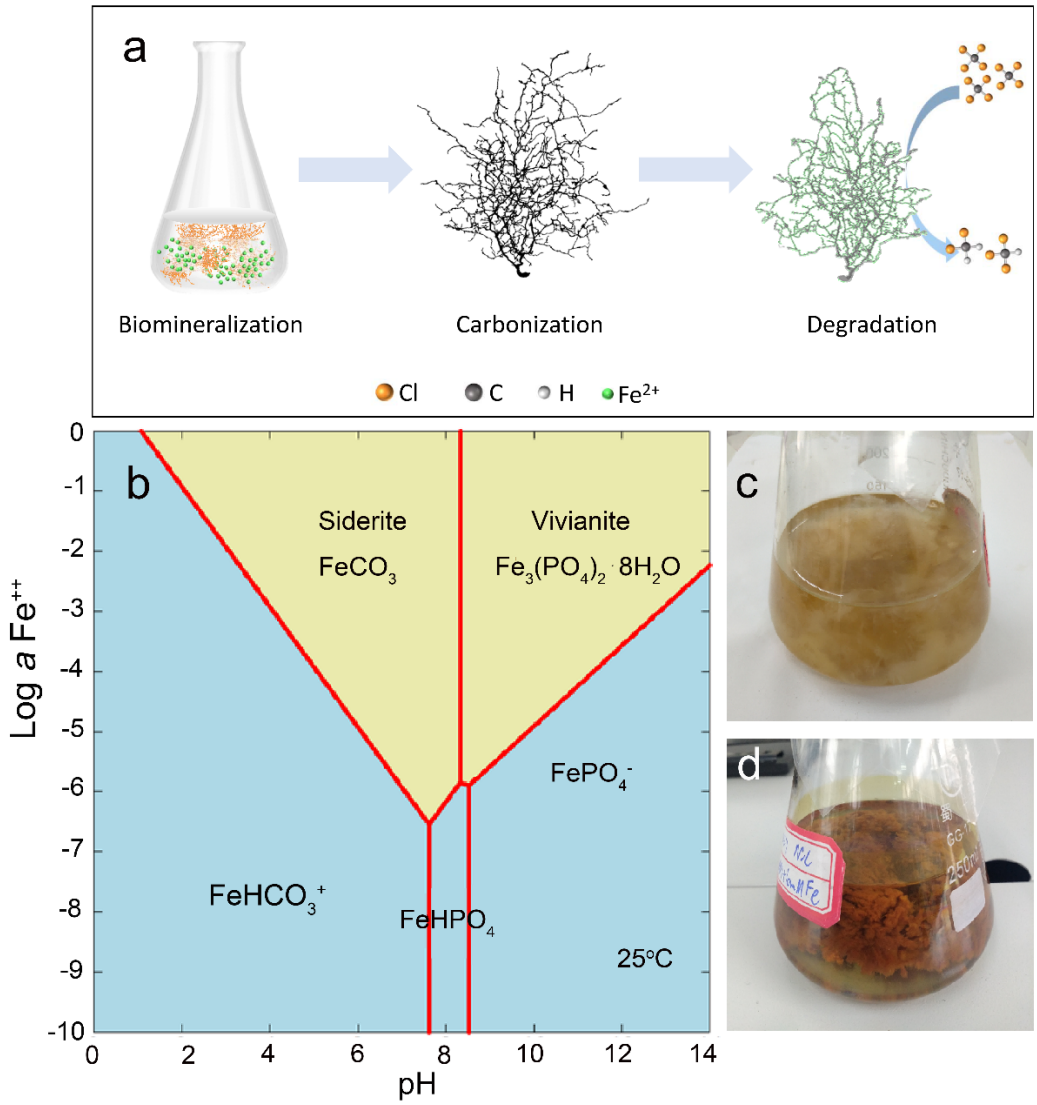

157

158 **Figure 1.** (a) Schematic illustration of the synthesis of nano zerovalent iron with a unique N-
159 doped branching structure. (b) Solubility diagram of Fe^{2+} versus pH at 25°C in a geochemically
160 simulated medium containing 0.33 M CO_3^{2-} after incubation with *N. crassa*. Chemical
161 parameters of the simulated system were set at 0.33 M CO_3^{2-}, 6.1 mM Cl^-, 0.83 mM SO_4^{2-}, 0.66
162 M NH_4^+, 4 mM K^+, 0.8 mM Mg^{2+}, 1.7 mM Na^+, 0.2 mM Ca^{2+}, 0.02 mM Mn^{2+}, 0.01 Mm Zn^{2+}
163 and 9 μm Fe^{3+}. The symbol *a* on the y-axis represents the effective concentration of a given
164 chemical species in a mixture. (c) Images of *N. crassa* grown in control AP1 liquid medium or
165 (d) AP1 containing 10 mM Fe^{2+} for 6 d at 25°C in the dark. Typical images are shown from
166 many similar examples.

After 6 d incubation, fungal biomass in control medium was pale yellow and flocculent (cotton wool-like) (Fig. 1c) while in Fe-modified AP1 medium, the fungal biomass tended to aggregate and yellow minerals were precipitated around the hyphae as well as in the medium (Fig. 1d), the colour changes clearly visible to the naked eye. The SEM results showed that the fungal hyphae were enveloped by a compact layer of minerals (Fig. 2a). This mineral sheath was comprised of granular nanoscale particles (~80 nm) (Fig. 2b) and the main elements detected in the minerals were C, O and Fe (Fig. 2a) which suggested formation of iron carbonates and oxides according to previous experiments [22].

After the carbonization and reduction process (heat treatment at 900^{o}C), the surface of the fungal hyphae became porous with individual nanoparticles (~50 nm) adhering to the carbonized hyphae, resulting in a coralline appearance, for which we designated the epithet 'iron coral' (Fig. 2c, d). EDXA analysis showed that C and Fe were the main elements in the 'iron coral' and little O was detected (Fig. 2c). At the higher concentration of Fe^{2+} (20 mM), more minerals were precipitated around the hyphae and after the heat treatment, the Fe-containing mineral sheath was still compact (Fig. 2e,f) but the mineral particles attached to the hyphae were larger (200~300 nm) than those forming at the lower concentration of Fe^{2+} (10 mM) (Fig. 2d,f). To further confirm the location and distribution of iron within the biominerals after heat treatment, X-ray mapping was carried out. It was found that iron was distributed evenly around the carbonized fungal hyphae (Fig. S1). Simple qualitative analysis from EDXA estimated that the amount of Fe was around 40% while carbon and oxygen were 45% and 15%, respectively.

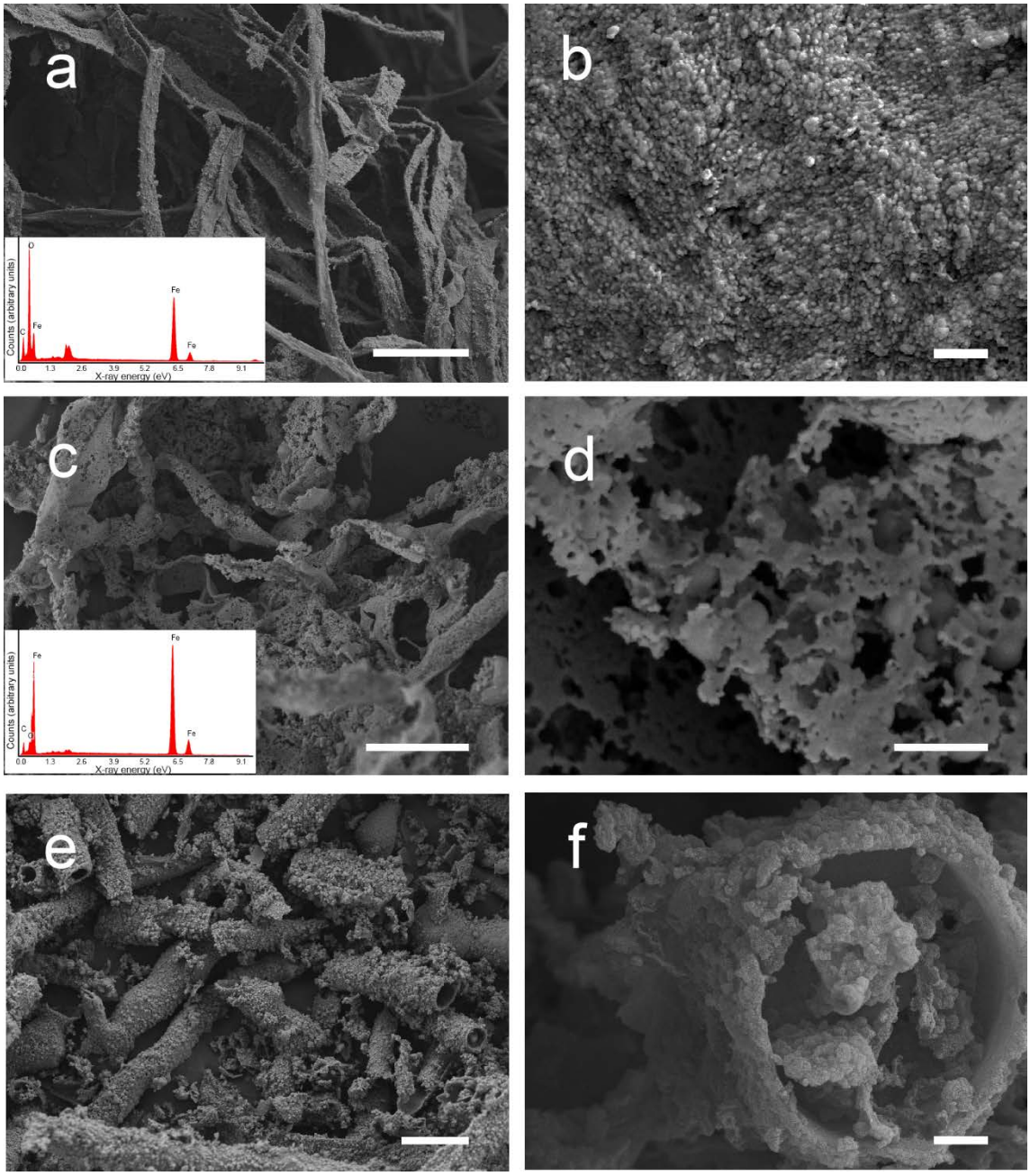

188

189 **Figure 2.** Scanning electron microscopy (SEM) and elemental analysis of minerals precipitated
190 by *N. crassa* in Fe-modified media. Images are (a, b, e) before and (c, d, f) after biomass
191 carbonization at 900°C under nitrogen gas for 1 h. Insets show X-ray energy dispersive analysis
192 (EDXA) of the minerals precipitated by *N. crassa* (a) before and (c) after carbonization. Scale
193 bars: (a) = 20 μm, (b, d) = 400 nm, (c, e) = 10 μm, (f) = 600 nm. *N. crassa* was incubated with
194 (a-d) 10 mM, or (e, f) 20 mM Fe^{2+} for 12 d at 25°C in the dark. Typical images and spectra are
195 shown from many similar examples.

196 XRD showed that minerals precipitated by *N. crassa* grown in Fe-modified medium were
197 amorphous (Fig. 3a), precluding accurate identification, which might be due to the
198 bioprecipitation process being influenced by extracellular metabolites (e.g. protein, peptides,
199 polysaccharide, amino acids) [23]. FTIR spectroscopy was further applied for identification of
200 the biominerals precipitated (Fig. 3b). The broad absorption band at 3425 cm^{-1} was related to
201 the O-H stretching vibrations arising from hydroxyl groups in water. The bands at 2920 and
202 2850 cm^{-1} were due to C-H stretching corresponding to organic matter [26] in biomass.
203 Previous experiments have demonstrated that peaks in the region of 1660 to 1381 cm^{-1} were
204 attributable to the ν_3 vibrational mode of the carbonate ion, while the peaks at 1074 and 1034
205 cm^{-1} are due to the ν_1 vibrational mode of CO_3^{2-}. The adsorption band at 588 cm^{-1} can be
206 assigned to the vibrations of Fe-O which refers to iron oxide [27, 28]. Compared with the
207 EDXA results, it can be concluded that the biominerals precipitated were a mixture of hydrated
208 iron carbonate with trace amounts of iron oxides and ferric hydroxide (the latter according to
209 the medium colour) which was consistent with the geochemical simulation results. After the
210 900^oC heat treatment under a nitrogen atmosphere, the composite of fungal biomass and iron-
211 containing minerals (from medium containing 10 mM Fe) was identified as a mixture of
212 zerovalent iron (Fe^0), carbon iron ($Fe_{1.91}C_{0.09}$) and iron oxide (Fe_3O_4) (Fig.3c) which was
213 consistent with the EDXA results (Fig. 2c). Therefore, after heat treatment, a mixture of
214 carbonized fungal biomass with nanoscale zerovalent iron ('iron coral') was achieved. The
215 existence of trace amount of oxides might due to the subsequent oxidation of Fe^0 on the surface.
216 To further investigate the formation process of 'iron coral', TGA was applied to analyse the
217 thermal stability of prepared biogenic iron-containing minerals and fungal biomass before heat
218 treatment (Fig. 3d). The main weight loss for fungal biomass and biogenic iron-containing
219 minerals below 120^oC can be attributed to the release of free water or structural water [29].
220 There were several thermal events occurring from 140-300^oC which corresponded to

crystallization from the amorphous phase and subsequent decomposition of carbonates to oxides (Fig.3a, c). The peak at 358°C could be assigned to reduction of the iron oxide to zerovalent iron which was verified by the XRD results (Fig. 3c). For the fungal biomass, a series of events occurred with increasing temperature and the biomass dehydrated (below 130°C) and then carbonized gradually from 130 to 341°C.

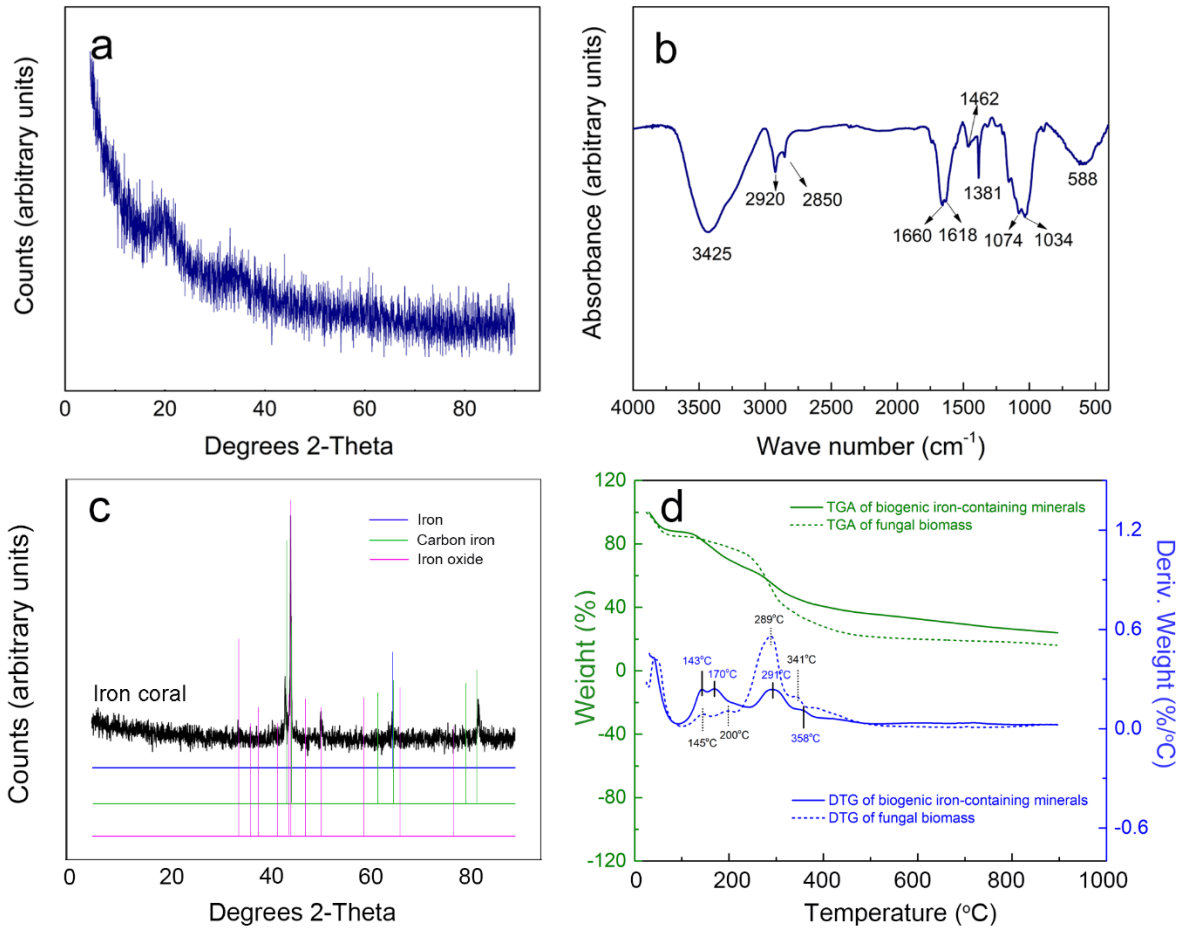

Figure 3. Characteristics of minerals precipitated by *N. crassa*. (a) X-ray diffraction (XRD) and (b) infrared spectroscopy (IR) of iron-containing minerals precipitated before carbonization and iron reduction. (c) XRD of minerals precipitated by *N. crassa* after carbonization and reduction at 900°C for 1 h. *N. crassa* was cultured in AP1 liquid medium amended with 10 mM Fe^{2+} for 6 d at 25°C in the dark. (d) Thermogravimetric analysis (TGA) and derivative thermogravimetric (DTG) curves of biogenic iron-containing minerals and fungal biomass under nitrogen at a heating rate of 5°C min^{-1}. Green and blue lines refer to TGA

and DTG, respectively. Solid and dashed lines are for iron-containing minerals and fungal biomass, respectively. Typical patterns and curves are shown from one of several determinations.

XPS was employed to investigate the surface chemical properties of 'iron coral'. The fully scanned spectrum of the sample showed five main peaks, at 977.1 eV, 716.3 eV, 530.7 eV, 400 eV and 283.9 eV, corresponding to O KLL, Fe 2p, O 1s, N 1s and C 1s, respectively (Fig. 4a). Four characteristic peaks were identified in the Fe 2p region, and the XPS spectrum for Fe $2p_{3/2}$ and Fe $2p_{1/2}$ core levels showed binding energies of 724.6 eV and 710.5 eV, respectively, which refer to Fe_2O_3 [30-32] (Fig. 4b). The peaks at 719.4 and 707.8 eV indicated the presence of carbon iron and elemental iron (Fe^0) on the surface, respectively [30]' . The peak at 712.7 eV represents the oxidized state of FeOOH.[32, 33]. The O 1s spectrum fitted with three components at 529.8, 531.1 and 532.2 eV, which correspond to oxide oxygen, hydroxyl groups and adsorbed water, respectively.[30, 32] (Fig. 4c). The presence of iron oxide suggested that the freshly prepared nano zerovalent iron was still partially oxidized. The XPS C 1s spectrum could be deconvoluted into four components, including C-Fe (283.8 eV), C-C (284.5 eV), C-H (285.6 eV), and C-O (286.6 eV) [28, 34] (Fig. 4d).

Pore size distributions of the carbonized fungal biomass and 'iron coral' composite were evaluated through N_2 adsorption/desorption isotherms (Fig. S2). Both samples exhibited a type IV isotherm with type H4 hysteresis loops, indicating a typical microporous and mesoporous structure in accordance with the IUPAC classification [30, 35]. The BET surface area of carbonized fungal biomass and iron coral were calculated to be 289.3 and 160.4 $m^2\ g^{-1}$, respectively. In terms of pore size distribution, both carbonized fungal biomass and 'iron coral' displayed a multimodal pore size distribution with the pore sizes being less than 100 nm diameter.

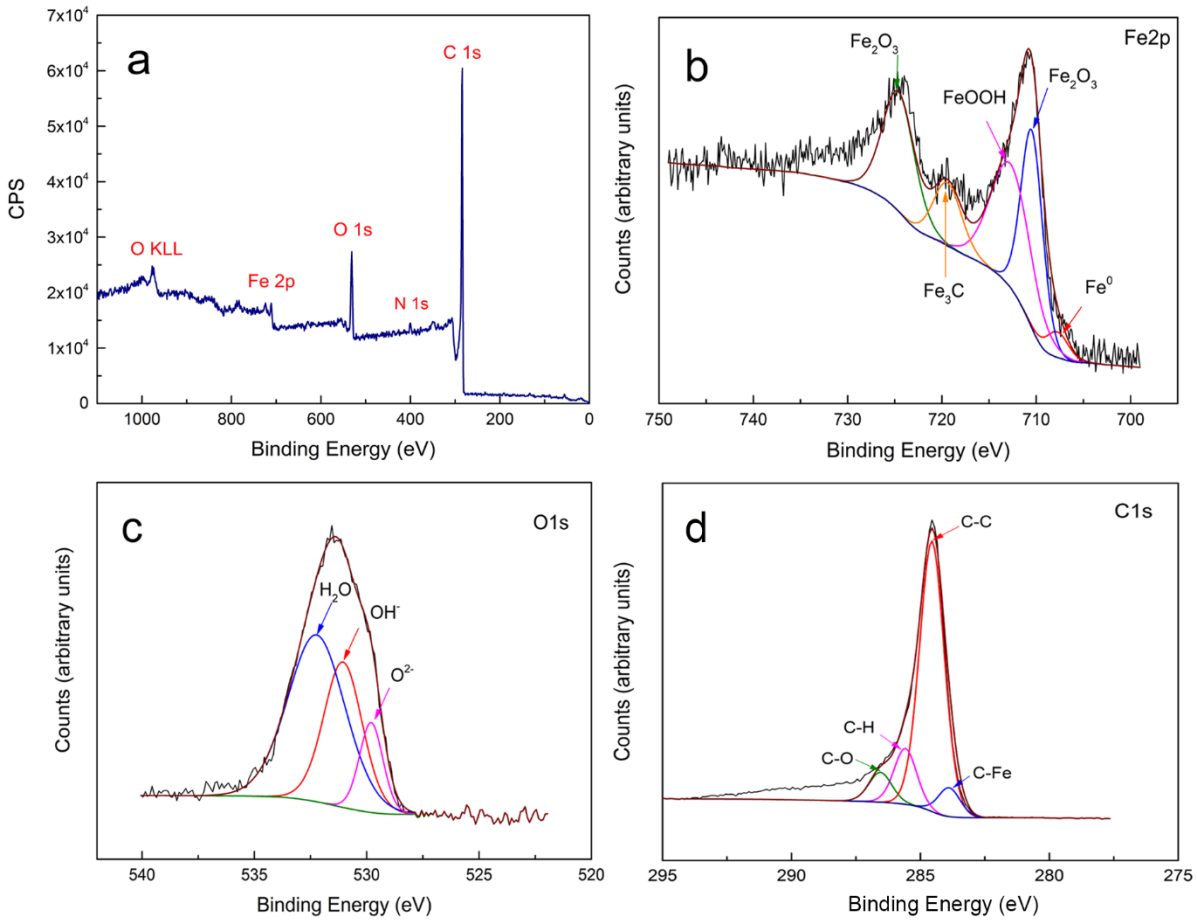

Figure 4. (a) X-ray photoelectron spectroscopy (XPS) survey spectrum for the 'iron coral' composite and high resolution XPS spectra of (b) Fe 2p, (c) O 1s and (d) C 1s. A typical pattern and spectra are shown from one of several determinations.

3.2 Stability of the iron coral composite

The migration of biomineralized iron coral in an aqueous solution was conducted to evaluate stability (Fig. 5a, d, g) and the zeta potential measurements for iron coral are shown in Fig.S3. Once mixed with water, the carbonized fungal biomass dispersed into different layers due to weight differences while the iron coral composite and commercial nZVI distributed evenly in the solution within the first 10 s (Fig. 5b, e, h). However, both the carbonized fungal biomass and commercial nZVI subsequently settled with the solution clearing and becoming transparent

while the solution containing ‘iron coral’ remained dark (Fig. 5c, f, i) which illustrated its nanoparticulate nature, and properties of enhanced mobility and dispersability. To further investigate the stability and mobility of the iron coral composite, stability analysis was applied using a LUMi X-Ray Reader during the sedimentation process (Fig. 6). The different coloured curves represent the intensity of transmitted light from the meniscus to the vessel bottom at selected time intervals. The first red line at the bottom represents the intensity of transmitted light over the first 10 s. Except for the cell bottom, the transmitted light intensity of the cell with iron coral (Fig. 6b) and fungal biomass (Fig. 6c) increased gradually within 1 h (Fig. 6b). The sedimentation process of the iron coral composite was more stable and the transmitted light increased gradually from 45% to 60% (except over the first 10 s). For the fungal biomass, the sedimentation behaviour depended on its position: the sedimentation rate of the sample in the upper layer of the cell was rapid while the sample in the lower layer sedimented slowly (Fig. 6c) which may be due to size differences in the fungal biomass. The intensity of the cell containing commercial nZVI (Fig. 6d) decreased significantly and blocked the transmitted light which indicated the rapid sedimentation of these particles. These results clearly showed that the stability of the iron coral composite in aqueous solution was better than fungal biomass alone and commercial nZVI particles.

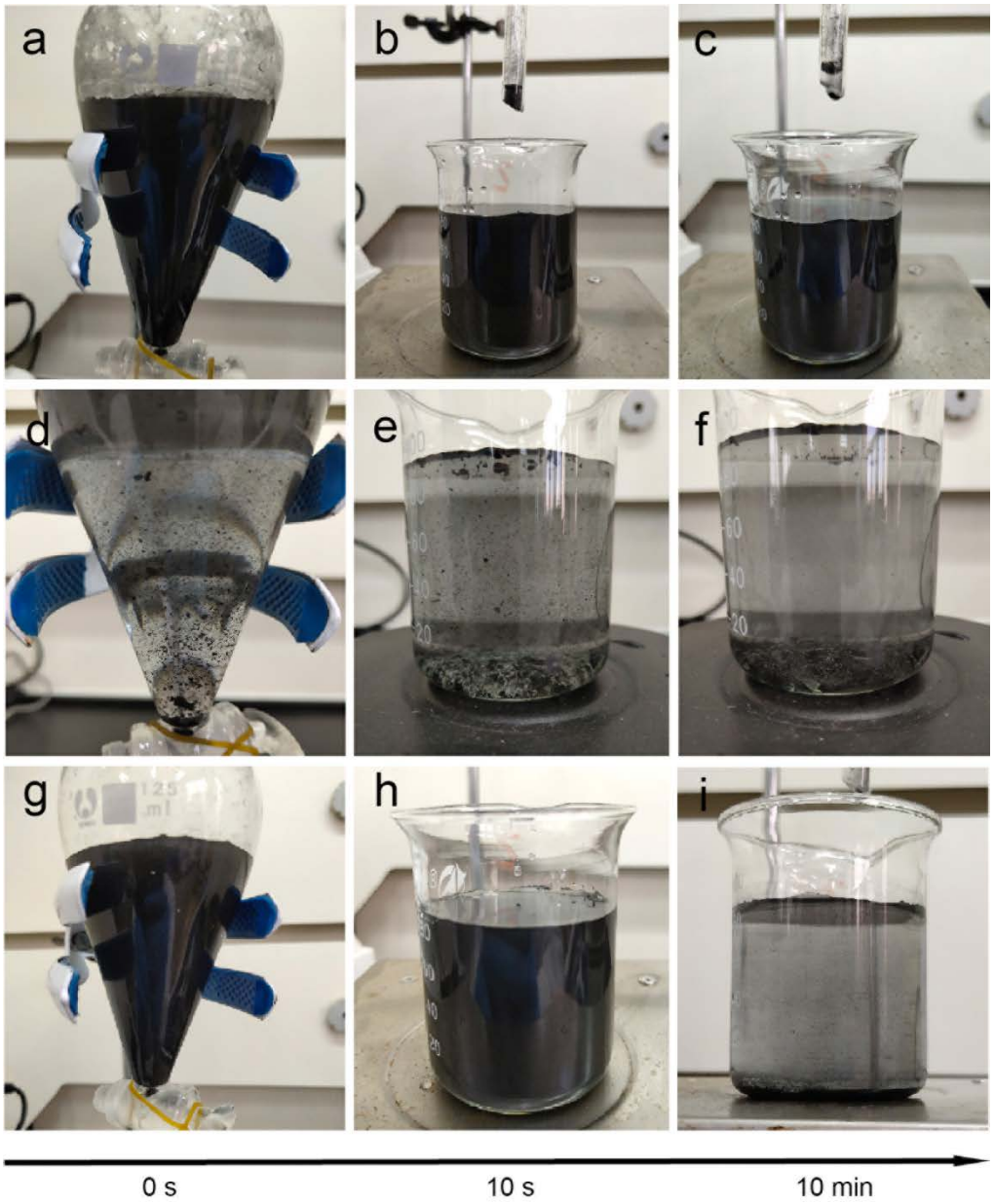

289

290 **Figure 5.** Mobility of (a-c) iron coral composite, (d-f) carbonized fungal biomass and (g-i)
291 commercial nZVI in water at different time periods. The concentration of the solid materials
292 was 1 g L^{-1} (dry weight). Typical images are shown from many similar samples.

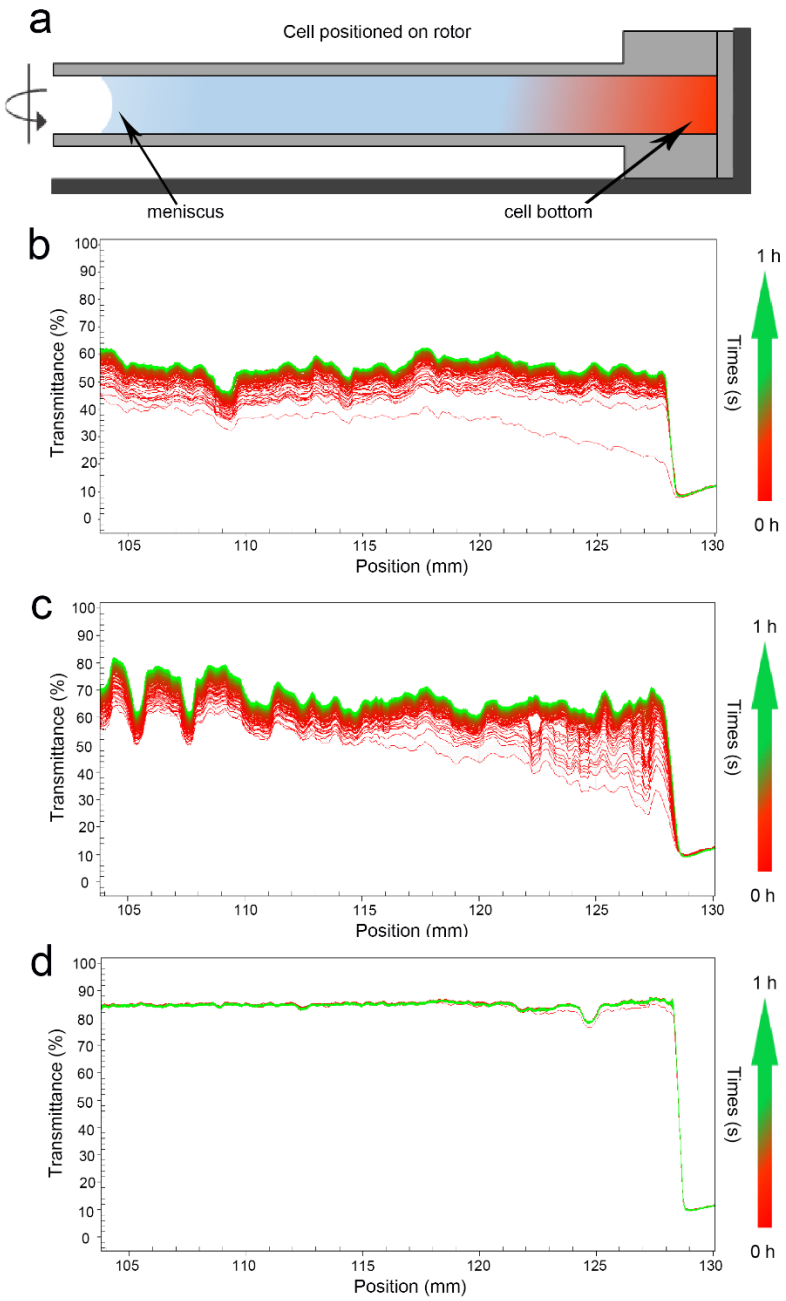

293

294 **Figure 6.** Evolution of time dependent transmission profiles of iron coral, zerovalent iron or
295 fungal biomass suspension. (a) Diagram of the measurement principle of the Stability Analyser.
296 (b) iron coral composite, (c) carbonized fungal biomass, (d) commercial nano zerovalent iron.
297 Different coloured curves represent the intensity of transmitted light from the meniscus to the
298 bottom of the vessel at different scan times. Profiles were taken every 10 s at 1000 rpm over 1
299 h.

3.3 Removal of carbon tetrachloride by iron coral

The performance of iron coral (obtained using 10 mM Fe^{2+}), carbonized fungal biomass and commercial nZVI was evaluated for the removal of carbon tetrachloride (CCl_4) from aqueous solution. The three solid sample materials (0.1 g) were mixed with CCl_4 (16 mg L^{-1}) and the concentration of CCl_4 in solution was measured at 30 min intervals. After 150 min reaction, the concentration of CCl_4 decreased to different levels: the iron coral composite showed the highest removal rate of around 75% while only 40% of CCl_4 was removed by carbonized fungal biomass and 66% of CCl_4 was removed by commercial nZVI (Table 1). To further investigate the intermediate degradation products during the reaction with iron coral, the aqueous solution was analyzed at 30 min intervals. It was found that the main product detected was CCl_4 with trace dichloromethane (CH_2Cl_2) and little trichloromethane ($CHCl_3$) being detected (Fig. 7a). Concomitant with the decrease of CCl_4 in solution, the amount of CH_2Cl_2 increased gradually with time (Fig.7b-d). The concentration of Cl^- in the aqueous solution also increased with time (data not shown).

Table 1 Concentrations of CCl_4 in solution after reaction with iron coral, carbonized fungal biomass or commercial nZVI.

	Concentration of CCl_4 (mg l^{-1}) in solution after different reaction times (min)						Proportion of CCl_4 removed (%)
	0	30	60	90	120	150	
Iron coral composite	10.77±0.00	6.18±0.69	5.21±0.98	3.33±0.39	3.60±0.20	2.73±0.30	74.7
Carbonized fungal biomass	10.77±0.00	13.72±3.07	10.26±2.90	7.16±1.07	7.53±1.09	6.45±0.52	40.1
Commercial nZVI	11.67±0.00	10.34±2.03	9.71 ± 0.47	7.40±0.87	5.50±0.64	3.97±0.03	66.0

To further investigate the degradation kinetics of CCl_4 by iron coral, the concentrations of CCl_4 in solution over reaction time were analyzed, the blue dots showing the experimental data and the red line representing the simulated data (Fig. 7e). The results showed that the kinetics of degradation by iron coral can be described as a pseudo-first-order kinetic reaction (eq. 1.1):

$$\ln(C_t/C_0) = -k_{obs}\, t \qquad (1.1)$$

$$y = C_0\, e^{-k_{obs}x} \qquad (1.2)$$

$$y = 10.038\, \mathrm{e}^{-0.01x} \qquad (1.3)$$

Here, C_t was the concentration of CCl_4 remaining in solution after reaction, C_0 is the initial concentration of CCl_4 in the simulated model, k_{obs} is the first-order rate constant and t is the reaction time. The relation between the concentration of CCl_4 remaining in solution (y) and reaction time (x) can be described by equation 1.2 in Fig. 7e. In this experiment, the initial concentration of CCl_4 in the simulated model was calculated as 10.038 mg L^{-1}, k_{obs} was -0.01 and R^2 was 0.9098 (eq.1.3), which shows that the experimental data fitted very well with the simulated model and the degradation kinetics of CCl_4 followed a pseudo-first-order model.

To unravel the reasons for the CCl_4 degradation ability of iron coral, the electron transfer properties of iron coral were checked using a Tafel scan technique which was used to measure free corrosion potentials (Fig. 7f). The results showed that the free corrosion potentials for iron coral and commercial nZVI were -0.76 and -0.84 V, respectively. The lower free corrosion potential of the sample is easily recognized to reflect corrosion, which indicates a higher ability to lose electrons. This 80 mV gap in the free corrosion potentials between iron coral and commercial nZVI suggested that electron release from iron coral was faster than that from commercial nZVI, and this contributed to the superior CCl_4 degradation performance of the iron coral.

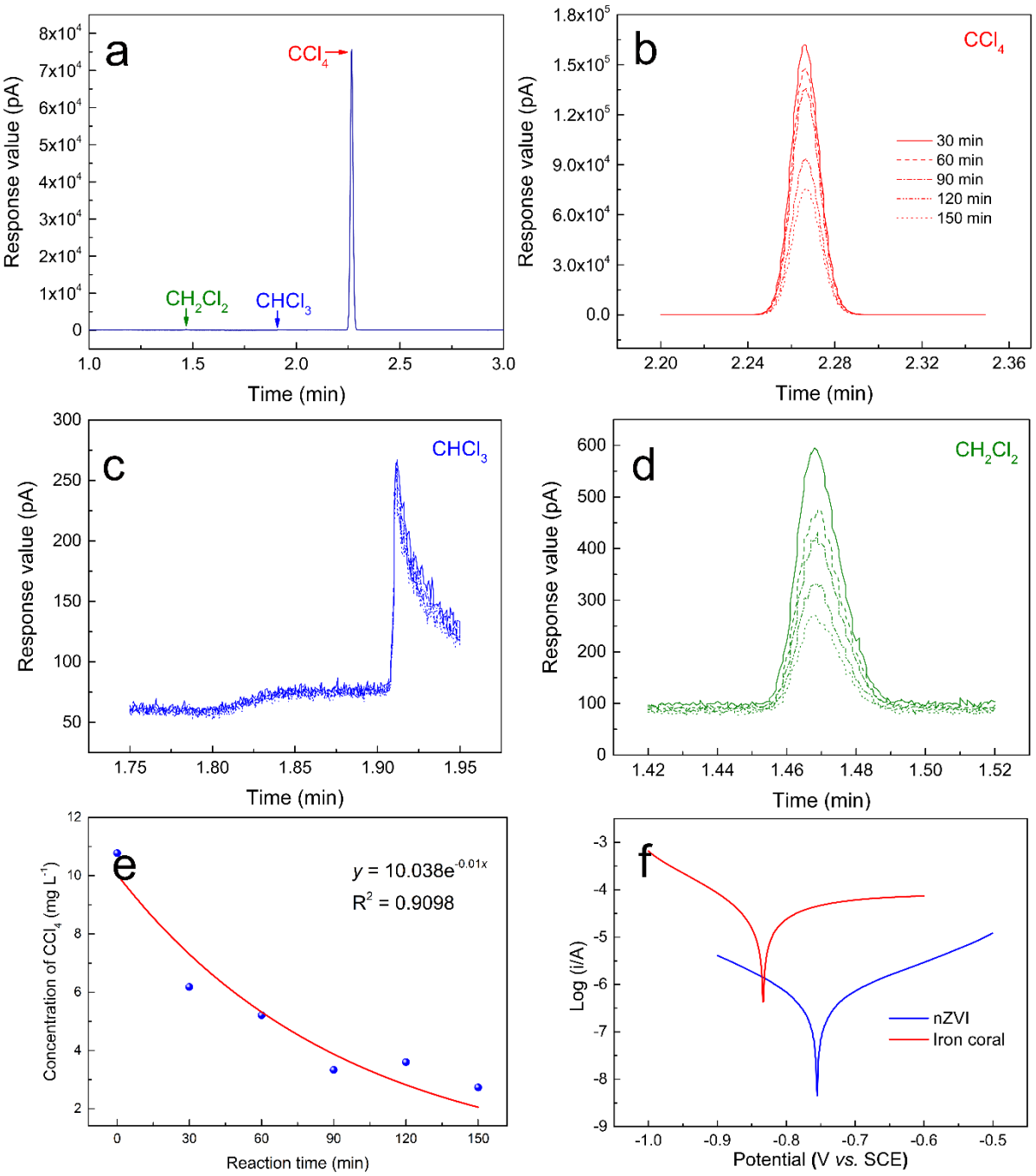

341

342 **Figure 7.** Formation of degradation products in solution over reaction time with iron coral. (a)
343 Products detected after 50 min and changes in the relative amounts of (b) CCl_4, (c) $CHCl_3$, (d)
344 CH_2Cl_2 in solution according to changes in peak intensity. (e) Kinetics of CCl_4 degradation by
345 the iron coral composite and (f) Tafel scans of iron coral and commercial nZVI in 0.5 mol L^{-1}
346 $NaSO_4$ solution. Typical chromatograms are shown from one of several determinations.

4. Discussion

Nanosized zerovalent iron nZVI has been widely investigated for the remediation or reductive dechlorination of chlorinated solvents from contaminated sites due to its high reactivity with contaminants and mobility in porous media [36-38]. However, the major technical challenge for preparing nZVI particles is to prevent aggregation and develop stabilized nZVI through appropriate surface modification technology and/or creating a network with an additional stabilizer (e.g. polymers, surfactants, silica) that separates the nanoparticles [39]. Not all those methods are applicable for preparation of nZVI and some polymers may not function properly in the aqueous phase while some stabilizers may cause secondary contamination. In this research, a fungal biomineralization process was used for the synthesis of nZVI. The biogenic nZVI distributed evenly around the fungal hyphae which we have termed 'iron coral' according to the morphology and the precipitation process. The biogenic iron coral showed an excellent removal capacity for CCl_4 (~75%) compared with carbonized fungal biomass or a commercial nZVI product.

Previous research has demonstrated that ureolytic fungi grown in urea-modified medium provide a promising method for the biomineralization of metal-containing minerals including carbonates, e.g. $CaCO_3$, $SrCO_3$, $MnCO_3$, and oxides (MnO, Mn_2O_3), especially those in the nanoscale [18, 19, 23]. The process of biomineralization refers to the formation of minerals by organisms and the final products may contain both minerals and organic components. Biomineralization processes include biologically-induced mineralization (BIM) and biologically-controlled mineralization (BCM). The formation of a coral skeleton is representative of BCM, which can be described as a protein controlling the process of mineral crystallization with the organic matrix controlling and influencing the biomineralization process and end-stage densification [40]. For the BIM process, e.g. ureolytic fungi incubated in urea and Fe^{2+}-supplemented medium, degradation of urea and the release of carbonate

increases the pH of the microenvironment, and results in the precipitation of iron carbonate. The geochemical simulation of iron and carbonate speciation in the reaction system matched very well with the experimental data. The filamentous hyphae were surrounded by iron-containing minerals and after heat treatment, the iron nanoparticles (derived from the reduction of iron oxide by fungal biomass carbonization) were distributed evenly around the carbonized hyphae which resembled coral decorated with iron particles. Previous research has demonstrated that the conformation of extracellular proteins can play an important role in the fungal precipitation of nanoscale minerals [23], which is analogous to the formation of natural coral, hence 'iron coral'. Compared with carbonized fungal biomass, the BET surface area of biogenic iron coral was lower (160.4 m^2 g^{-1}) which may be due to the nZVI being embedded in the fungal biomass and blocking the porous structure. This is consistent with findings for a nZVI synthesised through the reduction of Fe^{3+} by $NaBH_4$ solution and supported by reductive graphene oxides [41].

The stability of the iron coral composite was much better than the carbonized fungal biomass and commercial nZVI. Stability is one of the most important factors determining degradation ability in the aqueous phase. When mixed with CCl_4 solution (16 mg L^{-1}), little sedimentation occurred in the mixture containing the iron coral composite, which may be one of the reasons that the iron coral composite showed higher CCl_4 degradation ability (75%) than that of carbonized fungal biomass and commercial nZVI. Some previous research has been carried out on the degradation of chlorinated organic compounds by nZVI. Formic acid was applied to enhance the degradation of CCl_4 (2 mg L^{-1}) by nZVI and the degradation efficiency increased from 11.4% to 85% [42], while the CCl_4 (2 mg L^{-1}) removal efficiency of nZVI assembled on the surface of Fe_3O_4 was around 66% [43]. Most of the obtained kinetic data fitted to a pseudo-first-order kinetic model [43-46]. Ma et al. [47] reported that 94% of CCl_4 (3 mg L^{-1}) could be efficiently removed from aqueous solution by nanoscale palladized zero-valent iron-graphene

composites and that the degradation kinetics followed pseudo first-order reaction kinetics. Here, the dispersibility of nZVI was significantly improved by the graphene due to the larger specific surface area. In this experiment, the degradation kinetics of CCl_4 well fitted a pseudo-first-order reaction model, which was consistent with our reported findings. Moreover, the lower free corrosion potentials of iron coral composites (-0.84 V) indicated a higher ability to lose electrons, with the nitrogen in the fungal biomass inducing defects in the carbon framework which will also increase electron delocalization [48], thereby resulting in higher degradation of CCl_4. This work shows that biogenic iron coral is an efficient and highly promising candidate for the removal of chlorinated hydrocarbon pollutants from aqueous solution. Furthermore, fungi are effective biosorbents for metal ions and the origin of Fe^{2+} could be from, e.g. electroplating or mining wastewaters.

5. Conclusions

In this study, fungal biomineralization provided a facile method for the synthesis of nanoscale zerovalent iron (nZVI) showing a unique N-doped branching structure. Compared with commercial nZVI and carbonized fungal biomass, the iron coral composite showed excellent stability and mediated high degradation of carbon tetrachloride (~75%). The growth of ureolytic fungi in urea-containing media therefore provides a promising system for novel preparation of nZVI through a biomineralization process, with the iron coral nZVI/carbonized biomass showing significant potential for chlorinated pollutant removal from solution as well as metal recovery.

Acknowledgments

This work was supported by the National Natural Science Foundation of China (Grant No.41701352); the Open Project Program of the State Key Laboratory of Petroleum Pollution

Control (Grant No. PPC2019012); and the National Key R&D Program of China (No. 2018YFC1801903-01). GMG gratefully acknowledges financial support of the Geomicrobiology Group from the Natural Environment Research Council, UK (NE/M010910/1 (TeaSe); NE/M011275/1 (COG^3)).

References

[1] J. Yang, L. Meng, L. Guo, In situ remediation of chlorinated solvent-contaminated groundwater using ZVI/organic carbon amendment in China: field pilot test and full-scale application, Environmental Science and Pollution Research 25 (2018) 5051-5062.

[2] M. Stefaniuk, P. Oleszczuk, Y.S. Ok, Review on nano zerovalent iron (nZVI): from synthesis to environmental applications, Chemical Engineering Journal 287 (2016) 618-632.

[3] P. Wanner, B.L. Parker, S.W. Chapman, R. Aravena, D. Hunkeler, Quantification of degradation of chlorinated hydrocarbons in saturated low permeability sediments using compound-specific isotope analysis, Environmental Science & Technology 50 (2016) 5622-5630.

[4] S. Chen, J. Bedia, H. Li, L.Y. Ren, F. Naluswata, C. Belver, Nanoscale zero-valent iron@mesoporous hydrated silica core-shell particles with enhanced dispersibility, transportability and degradation of chlorinated aliphatic hydrocarbons, Chemical Engineering Journal 343 (2018) 619-628.

[5] X. Guan, Y. Sun, H. Qin, J. Li, I.M.C. Lo, D. He, H. Dong, The limitations of applying zero-valent iron technology in contaminants sequestration and the corresponding countermeasures: the development in zero-valent iron technology in the last two decades (1994–2014), Water Research 75 (2015) 224-248.

[6] M. Mangayayam, K. Dideriksen, M. Ceccato, D.J. Tobler, The structure of sulfidized zero-valent iron by one-pot synthesis: impact on contaminant selectivity and long-term performance, Environmental Science & Technology 53 (2019) 4389-4396.

[7] F. Fu, D.D. Dionysiou, H. Liu, The use of zero-valent iron for groundwater remediation and wastewater treatment: a review, Journal of hazardous materials 267 (2014) 194-205.

[8] R. Mukherjee, R. Kumar, A. Sinha, Y. Lama, A.K. Saha, A review on synthesis, characterization, and applications of nano zero valent iron (nZVI) for environmental

remediation, Critical Reviews in Environmental Science and Technology 46 (2016) 443-466.

[9] H. Dong, Q. He, G. Zeng, L. Tang, C. Zhang, Y. Xie, Y. Zeng, F. Zhao, Y. Wu, Chromate removal by surface-modified nanoscale zero-valent iron: effect of different surface coatings and water chemistry, Journal of colloid and interface science 471 (2016) 7-13.

[10] J. Soukupova, R. Zboril, I. Medrik, J. Filip, K. Safarova, R. Ledl, M. Mashlan, J. Nosek, M. Cernik, Highly concentrated, reactive and stable dispersion of zero-valent iron nanoparticles: direct surface modification and site application, Chemical Engineering Journal 262 (2015) 813-822.

[11] R. Fu, Y. Yang, Z. Xu, X. Zhang, X. Guo, D. Bi, The removal of chromium (VI) and lead (II) from groundwater using sepiolite-supported nanoscale zero-valent iron (S-NZVI), Chemosphere 138 (2015) 726-734.

[12] Y. Sun, C. Ding, W. Cheng, X. Wang, Simultaneous adsorption and reduction of U (VI) on reduced graphene oxide-supported nanoscale zerovalent iron, Journal of Hazardous materials 280 (2014) 399-408.

[13] M.A. Kumar, S. Bae, S. Han, Y. Chang, W. Lee, Reductive dechlorination of trichloroethylene by polyvinylpyrrolidone stabilized nanoscale zerovalent iron particles with Ni, Journal of Hazardous Materials 340 (2017) 399-406.

[14] Y. Zou, X. Wang, A. Khan, P. Wang, Y. Liu, A. Alsaedi, T. Hayat, X. Wang, Environmental remediation and application of nanoscale zero-valent iron and its composites for the removal of heavy metal ions: a review, Environmental Science & Technology 50 (2016) 7290-7304.

[15] H. Chen, Y. Cao, E. Wei, T. Gong, Q. Xian, Facile synthesis of graphene nano zero-valent iron composites and their efficient removal of trichloronitromethane from drinking water, Chemosphere 146 (2016) 32-39.

[16] M. Velimirovic, H. Chen, Q. Simons, L. Bastiaens, Reactivity recovery of guar gum coupled mZVI by means of enzymatic breakdown and rinsing, Journal of Contaminant

Hydrology 142 (2012) 1-10.

[17] Q.W. Li, L. Csetenyi, G.M. Gadd, Biomineralization of metal carbonates by *Neurospora crassa*, Environmental Science & Technology 48 (2014) 14409-14416.

[18] Q. Li, G.M. Gadd, Fungal nanoscale metal carbonates and production of electrochemical materials, Microbial Biotechnology 10 (2017) 1131-1136.

[19] Q. Li, L. Csetenyi, G.I. Paton, G.M. Gadd, $CaCO_3$ and $SrCO_3$ bioprecipitation by fungi isolated from calcareous soil, Environmental Microbiology 17 (2015) 3082-3097.

[20] G.M. Gadd, Geomicrobiology of the built environment, Nature Microbiology 2 (2017) No 16275.

[21] F. Liu, L. Csetenyi, G.M. Gadd, Amino acid secretion influences the size and composition of copper carbonate nanoparticles synthesized by ureolytic fungi, Applied Microbiology and Biotechnology 103 (2019) 7217-7230.

[22] Q. Li, D. Liu, Z. Jia, L. Csetenyi, Geoffrey M. Gadd, Fungal biomineralization of manganese as a novel source of electrochemical materials, Current Biology 26 (2016) 950-955.

[23] Q. Li, D. Liu, C. Chen, Z. Shao, H. Wang, J. Liu, Q. Zhang, G.M. Gadd, Experimental and geochemical simulation of nickel carbonate mineral precipitation by carbonate-laden ureolytic fungal culture supernatants, Environmental Science: Nano 6 (2019) 1866-1875.

[24] L. Krejčová, T. Leonhardt, F. Novotný, V. Bartůněk, V. Mazánek, D. Sedmidubský, Z. Sofer, M. Pumera, A metal-doped fungi-based biomaterial for advanced electrocatalysis, Chemistry – A European Journal 25 (2019) 3828-3834.

[25] Y. Hu, X. Peng, Z. Ai, F. Jia, L. Zhang, Liquid nitrogen activation of zero-valent iron and its enhanced Cr (VI) removal performance, Environmental Science & Technology 53 (2019) 8333-8341.

[26] A.K. Suresh, D.A. Pelletier, W. Wang, M.L. Broich, J.-W. Moon, B. Gu, D.P. Allison, D.C. Joy, T.J. Phelps, M.J. Doktycz, Biofabrication of discrete spherical gold nanoparticles using

the metal-reducing bacterium *Shewanella oneidensis*, Acta Biomaterialia 7 (2011) 2148-2152.

[27] B. Bajaj, B.D. Malhotra, S. Choi, Preparation and characterization of bio-functionalized iron oxide nanoparticles for biomedical application, Thin Solid Films 519 (2010) 1219-1223.

[28] J. Guo, R. Wang, W.W. Tjiu, J. Pan, T. Liu, Synthesis of Fe nanoparticles@graphene composites for environmental applications, Journal of Hazardous Materials 225-226 (2012) 63-73.

[29] C. Ding, W. Cheng, X. Nie, F. Yi, S. Xiang, A.M. Asiri, H.M. Marwani, Reactivity of carbonized fungi supported nanoscale zero-valent iron toward U(VI) influenced by naturally occurring ions, Journal of Industrial and Engineering Chemistry 61 (2018) 236-243.

[30] Y. Wang, H. Sun, X. Duan, H.M. Ang, M.O. Tadé, S. Wang, A new magnetic nano zero-valent iron encapsulated in carbon spheres for oxidative degradation of phenol, Applied Catalysis B: Environmental 172-173 (2015) 73-81.

[31] Y. Mu, F. Jia, Z. Ai, L. Zhang, Iron oxide shell mediated environmental remediation properties of nano zero-valent iron, Environmental Science: Nano 4 (2017) 27-45.

[32] H. Woo, J. Park, S. Lee, S. Lee, Effects of washing solution and drying condition on reactivity of nano-scale zero valent irons (nZVIs) synthesized by borohydride reduction, Chemosphere 97 (2014) 146-152.

[33] H.-S. Kim, T. Kim, J.-Y. Ahn, K.-Y. Hwang, J.-Y. Park, T.-T. Lim, I. Hwang, Aging characteristics and reactivity of two types of nanoscale zero-valent iron particles (FeBH and FeH_2) in nitrate reduction, Chemical Engineering Journal 197 (2012) 16-23.

[34] Z. Zhu, Y. Xu, B. Qi, G. Zeng, P. Wu, G. Liu, W. Wang, F. Cui, Y. Sun, Adsorption-intensified degradation of organic pollutants over bifunctional α-Fe@carbon nanofibres, Environmental Science: Nano 4 (2017) 302-306.

[35] P. Zhang, Y. Zhan, B. Cai, C. Hao, J. Wang, C. Liu, Z. Meng, Z. Yin, Q. Chen, Shape-controlled synthesis of Mn_3O_4 nanocrystals and their catalysis of the degradation of methylene

blue, Nano Research 3 (2010) 235-243.

[36] H. Dong, Z. Cong, K. Hou, Y. Cheng, G. Zeng, Removal of trichloroethylene by biochar supported nanoscale zero-valent iron in aqueous solution, Separation & Purification Technology 188 (2017) 188-196.

[37] T. Phenrat, T. Thongboot, G.V. Lowry, Electromagnetic induction of zerovalent iron (ZVI) powder and nanoscale zerovalent iron (nZVI) particles enhances dechlorination of trichloroethylene in contaminated groundwater and soil: proof of concept, Environmental Science & Technology 50 (2015) 872-880.

[38] H. Tian, Y. Liang, T. Zhu, X. Zeng, Y. Sun, Surfactant-enhanced PEG-4000-NZVI for remediating trichloroethylene-contaminated soil, Chemosphere 195 (2018) 585-593.

[39] X. Zhao, W. Liu, Z. Cai, B. Han, T. Qian, D. Zhao, An overview of preparation and applications of stabilized zero-valent iron nanoparticles for soil and groundwater remediation, Water Research 100 (2016) 245-266.

[40] D.W. Green, B. Ben-Nissan, K.S. Yoon, B. Milthorpe, H.-S. Jung, Natural and synthetic coral biomineralization for human bone revitalization, Trends in Biotechnology 35 (2017) 43-54.

[41] L. Jie, C. Changlun, Z. Rui, W. Xiangke, Nanoscale zero-valent iron particles supported on reduced graphene oxides by using a plasma technique and their application for removal of heavy-metal ions, Chemistry- An Asian Journal 10 (2015) 1410-1417.

[42] W. Jiang, D.D. Dionysiou, M. Kong, Z. Liu, Q. Sui, S. Lyu, Utilization of formic acid in nanoscale zero valent iron-catalyzed Fenton system for carbon tetrachloride degradation, Chemical Engineering Journal 380 (2020) 122537-122544.

[43] X. Lv, H. Li, Y. Ma, H. Yang, Q. Yang, Degradation of carbon tetrachloride by nanoscale zero-valent iron@magnetic Fe_3O_4: impact of reaction condition, kinetics, thermodynamics and mechanism, Applied Organometallic Chemistry 32 (2018) e4139.

[44] Y. Ma, X. Lv, Q.I. Yang, Y. Wang, X. Chen, Reduction of carbon tetrachloride by nanoscale palladized zero-valent iron@ graphene composites: kinetics, activation energy, effects of reaction conditions and degradation mechanism, Applied Catalysis A: General 542 (2017) 252-261.

[45] X.-F. Wan, C. Guo, Y. Liu, X.-S. Chai, Y. Li, G. Chen, Kinetic research on dechlorinating dichlorobenzene in aqueous system by nano-scale nickel/iron loaded with CMC/NFC hydrogel, Chemosphere 194 (2018) 297-305.

[46] L. Li, J. Hu, X. Shi, M. Fan, J. Luo, X. Wei, Nanoscale zero-valent metals: a review of synthesis, characterization, and applications to environmental remediation, Environmental Science and Pollution Research 23 (2016) 17880-17900.

[47] Y. Ma, X. Lv, Q. Yang, Y. Wang, X. Chen, Reduction of carbon tetrachloride by nanoscale palladized zero-valent iron@graphene composites: kinetics, activation energy, effects of reaction conditions and degradation mechanism, Applied Catalysis A: General 542 (2017) 252-261.

[48] Y. Zhou, L. Tang, G. Yang, G. Zeng, Y. Deng, B. Huang, Y. Cai, J. Tang, J. Wang, Y. Wu, Phosphorus-doped ordered mesoporous carbons embedded with Pd/Fe bimetal nanoparticles for the dechlorination of 2, 4-dichlorophenol, Catalysis Science & Technology 6 (2016) 1930-1939.